Spontaneously generated coherence effects in a laser-driven four-level atomic system

M. A. Antón, Oscar G. Calderón, and F. Carreño
Escuela Universitaria de Óptica, Universidad Complutense de Madrid, C/Arcos de Jalón s/n, 28037 Madrid, Spain
(Received 21 December 2004; revised manuscript received 12 April 2005; published 10 August 2005)

In this paper we investigate the resonance fluorescence, the squeezing, and the absorption spectra of a laser-driven four-level atom consisting of three closely spaced upper levels decaying to a common lower level. The three upper levels are coupled by the same vacuum modes to the lower level leading to spontaneously generated coherence effects. High population inversion and extremely narrow emission lines are obtained with moderate Rabi frequencies, which are a direct consequence of decay-induced interferences. The fluorescent field is shown to exhibit two-mode squeezing in the in-phase quadrature. Squeezing in both quadratures simultaneously at different frequencies is greatly enhanced when quantum interference is accounted for. We also examine the absorption spectrum of a weak field and demonstrate that quantum interference can induce two prominent and nearly transparent holes where the slope of the refractive index is very steep. This special situation could allow the simultaneous propagation of two weak pulses with different frequencies, which could be feasibly exploited towards the realization of the entanglement of two photons.

DOI: 10.1103/PhysRevA.72.023809 PACS number(s): 42.50.Gy, 32.80.−t

I. INTRODUCTION

Spontaneous emission of excited atoms is one of the fundamental processes in the interaction of radiation and matter. It is responsible for many important physical phenomena such as quantum noise of an optoelectronic device and it prevents the operation of a laser system at ultrashort wavelengths. For a long time one has desired to find an approach by which spontaneous emission of an excited atomic system can be depressed as much as possible or even canceled. Laser field induced quantum interferences have been proven to be crucial in controlling the optical properties of an atomic medium. Both stimulated processes such as light absorption and refraction [1,2] and also spontaneous processes were shown to be altered almost at will due to stimulated extra indistinguishable quantum-mechanical pathways [3,4]. Several theoretical proposals of atomic systems have appeared where coupling to one or more coherent fields allows the management of the optical properties [5]. Many interesting phenomena, such as electromagnetically induced transparency (EIT) [6,7], lasing without inversion (LWI) [8–11], refractive index enhancement without absorption [12–14], and giant nonlinearity [15–17] have been predicted and experimentally demonstrated and have modified the way we look at matter-radiation interactions.

The essential features of quantum interference processes are adequately covered by the three-level approximation (the so-called cascade, Λ, and V schemes). More recently, there has been considerable interest in coherent effects in multilevel systems since the presence of additional levels increases multifold the possibilities of interference phenomena to exist [18–21]. Schmidt and Imamoglu [22] and Grangier *et al.* [23] have proposed a four-level scheme in which giant Kerr nonlinearities and photon blockade may be obtained. Harris and Yamamoto and Harris and Hau have examined a four-level scheme that will absorb two photons but not one [24]. The experimental verification of this prediction has been carried out recently in a four-level atom using cold Rb atoms by Yan *et al.* [25]. Dark resonance switching among three-laser interactions in a four-level system has been observed by Ham and Hemmer [26] in rare-earth doped solids with applications to subpicosecond optical switches [27]. Other works include studies of coherent effects such as frequency up conversion [28] and the possibility of enhancing cross-phase modulation in such schemes [29]. In these systems, with an additional fourth atomic level in comparison to a Λ- or a V-type system, one of the ground levels undergoes an ac-Stark shift which disturbs the EIT resonance condition and can induce nonlinearities while keeping absorption negligible. The studies have predicted the ability to achieve an appreciable nonlinear phase shift using optical fields in the N configuration. It is worth mentioning that Lukin *et al.* [30] have recently proposed a mechanism to entangle two photons in an EIT medium based on obtaining slow photons at different frequencies. Since the EIT created in Λ or V atoms only provides the steep dispersion near the resonant frequency, sophisticated schemes are proposed to obtain slow photons at different frequencies [30–32]. For example, Lukin *et al.* [30] suggested the use of two species of atoms to obtain the matching of the group velocities of the interacting photons. Wang *et al.* [31] proposed the simultaneous use of two driving fields of different angular frequencies to slow down the photons, while Petrosyan and Kurizki [32] considered an N-type atom in a doped photonic band gap which allows the creation of entangled two-photon states. Here we show that EIT in a four level atom driven by a very weak field may be used to slow down photons at different frequencies when vacuum induced coherence is considered.

In some of the above-mentioned processes it is crucial to have at least three laser pulses to create the necessary coherences. However, coherence can be created and preserved via internal processes of the system, therefore requiring no coupling laser fields. In an early study, Agarwal [33] showed that an initially excited degenerate V-type three-level atom may not decay to its ground level due to the cancellation of spontaneous emission by quantum interference between the atomic transitions. If the two upper levels are very close and damped by the usual vacuum interactions, spontaneous emis-

sion cancellation can take place [34–37], which offers the possibility to trap population in the excited levels when some particular conditions hold [34–39]. Quantum interference between the two transition channels connecting the ground level is responsible for many interesting effects, such as narrow resonances and probe transparency [40–42], dark spectral lines [37,43], phase-dependent line shapes [44,45], gain features on dark transitions [46], vacuum-induced optical bistability [47,48], superradiance [49], gain without population inversion [50], among others.

In this paper we consider a four-level atom, where three closely lying levels are coupled via a single driving laser to a common lower state. In addition, we assume that the upper three levels interact with the same vacuum modes to decay to the ground level. The presence of three possibilities of arriving at the ground state from the excited levels can give rise to strong interference effects in the spectral correlation of the pairs of emitted photons. The same four-level atomic scheme used in the present work, was previously studied by Joshi *et al.* [51]. They analyzed the effect of spontaneously generated coherence on the spontaneous decay of population in the absence of driving fields, and they found that suppression of spontaneous decay becomes more significant as the number of upper levels participating in the spontaneous emission increases. The purpose of this work is twofold. First, we focus our attention on the influence of vacuum induced coherence on the resonance fluorescence spectrum and the squeezing spectrum. Second, we study the possibility of employing such a system to slow down light, which is attracting broad interest in view of its potentially impressive applications to quantum memories [52]. The most remarkable effect, which does not occur in the three-level V system, is that in the present scheme, a double transparency holes with adjustable frequencies in the absorption spectrum appear. In addition, a steeper dispersion occurs at these transparency windows. For suitable and controllable external parameters, the spectrum can be symmetrical, leading to the same group velocity at two different frequencies, so this atomic system can support the propagation of two weak pulses with the same group velocity at different central frequencies with the advantage that a single driving field of very weak intensity is required.

The paper is organized as follows: Section II establishes the model, i.e., the Hamiltonian of the system and the evolution equation of the atomic operators assuming the rotating wave approximation. Section III is devoted to present the numerical results and to discuss the effect of quantum interference on the population dynamics, the resonance fluorescence, the squeezing and the absorption spectra. Finally, Sec. IV summarizes the conclusions.

II. ATOMIC MODEL AND DENSITY-MATRIX EQUATIONS

We consider a four-level atom as shown in Fig. 1. It has three upper levels $|4\rangle$, $|3\rangle$, and $|2\rangle$, which are coupled by the same vacuum modes to the lower level $|1\rangle$. The spontaneous decay rates from the excited atomic levels $|4\rangle$, $|3\rangle$, and $|2\rangle$ to the ground level $|1\rangle$ are labeled as γ_4, γ_3, and γ_2, respectively. A coherent field is set to couple $|1\rangle$ to the three upper levels by choosing a frequency ω_L midway to the three-upper levels,

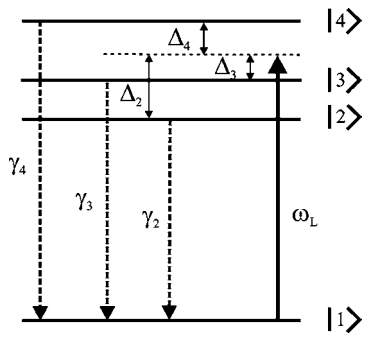

FIG. 1. A four-level atom driven by a single-mode laser of angular frequency ω_L. γ_4, γ_3, and γ_2 are the decay rates from the excited states $|4\rangle$, $|3\rangle$, and $|2\rangle$, to the ground level $|1\rangle$, respectively. Δ_i are the detunings of the driving field with the states $|i\rangle$ $(i=2,3,4)$.

$$\vec{E} = \frac{1}{2}\vec{E}_0 e^{-i\omega_L t} + \text{c.c.}, \tag{2.1}$$

$\vec{E}_0$ being the amplitude of the slowly varying field envelope. The resonant frequencies between the upper levels $|4\rangle$, $|3\rangle$, $|2\rangle$ and the ground level $|1\rangle$ are ω_{41}, ω_{31}, and ω_{21}, respectively. Note that $\omega_{i1}-\omega_{j1}=\omega_{ij}$, $\omega_{ij}(i\neq j\neq 1)$ being the frequency separation of the excited levels $|i\rangle$ and $|j\rangle$. The Hamiltonian of the system in the rotating wave approximation is given by [3,33]

$$H = \hbar\sum_{m=1}^{4}\omega_m\sigma_{mm} + \hbar\sum_{k\lambda}\omega_{k\lambda}b_{k\lambda}^{\dagger}b_{k\lambda} - \left[\hbar\sum_{m=2}^{4}\sum_{k\lambda}g_{mk}\sigma_{m1}b_{k\lambda} + \text{H.c.}\right] - \left[\hbar\sum_{m=2}^{4}\Omega_m e^{-i\omega_L t}\sigma_{m1} + \text{H.c.}\right], \tag{2.2}$$

where $\sigma_{mn}=|m\rangle\langle n|$ are the usual Pauli matrices, $\hbar\omega_m$ are the energies of the atomic levels, and $b_{k\lambda}$ $(b_{k\lambda}^{\dagger})$ is the annihilation (creation) operator of the kth mode of the vacuum field with polarization $\vec{e}_{k\lambda}$ $(\lambda=1,2)$ and angular frequency $\omega_{k\lambda}$. The parameter g_{mk} is the coupling constant of the atomic transition $|m\rangle\rightarrow|1\rangle$ with the electromagnetic vacuum mode

$$g_{mk} = \sqrt{\frac{\omega_{k\lambda}}{2\hbar\epsilon_0 V}}(\vec{\mu}_{1m}\cdot\vec{e}_{k\lambda}), \tag{2.3}$$

where $\vec{\mu}_{1m}$ is the dipolar moment of the transition, which is assumed to be real, and $\Omega_m=\vec{\mu}_{1m}\cdot\vec{E}_0/(2\hbar)$ is the Rabi frequency of the transition $|m\rangle\rightarrow|1\rangle$. The system is studied using the density-matrix formalism. By following the traditional approach of Weisskopf and Wigner [3,33], the equation of motion for the reduced density matrix in the interaction picture reads as

$$\frac{d\rho}{dt} = -\frac{i}{\hbar}[H_{ext},\rho] + \frac{1}{2}\mathcal{L}\rho, \tag{2.4}$$

where H_{ext} is the Hamiltonian and $\mathcal{L}$ is the Liouvillian of the system, which are given by

$$H_{ext} = \hbar \sum_{m=2}^{4} \Delta_m \sigma_{mm} + \hbar \sum_{m=2}^{4} (\Omega_m \sigma_{m1} + \text{H.c.}), \quad (2.5)$$

$$\begin{aligned}\mathcal{L} = {} & \gamma_4[2\sigma_{14}\rho\sigma_{41} - \sigma_{44}\rho - \rho\sigma_{44}] + \gamma_3[2\sigma_{13}\rho\sigma_{31} - \sigma_{33}\rho \\ & - \rho\sigma_{33}] + \gamma_2[2\sigma_{12}\rho\sigma_{21} - \sigma_{22}\rho - \rho\sigma_{22}] + \gamma_{42}[2\sigma_{14}\rho\sigma_{21} \\ & - \sigma_{24}\rho - \rho\sigma_{24}] + \gamma_{42}[2\sigma_{12}\rho\sigma_{41} - \sigma_{42}\rho - \rho\sigma_{42}] \\ & + \gamma_{43}[2\sigma_{14}\rho\sigma_{31} - \sigma_{34}\rho - \rho\sigma_{34}] + \gamma_{43}[2\sigma_{13}\rho\sigma_{41} - \sigma_{43}\rho \\ & - \rho\sigma_{43}] + \gamma_{32}[2\sigma_{13}\rho\sigma_{21} - \sigma_{23}\rho - \rho\sigma_{23}] + \gamma_{32}[2\sigma_{12}\rho\sigma_{31} \\ & - \sigma_{32}\rho - \rho\sigma_{32}], \end{aligned} \quad (2.6)$$

$\Delta_j = \omega_{j1} - \omega_L$, $(j=2,3,4)$ being the detunings of the field from the optical transitions and γ_j $(j=2,3,4)$ are the decay rates of the upper levels $|j\rangle$ to the ground level $|1\rangle$. The coefficients γ_{ij} are given by

$$\gamma_{ij} = \frac{\sqrt{\gamma_i \gamma_j}}{2} p_{ij}, \quad (j = 2,3,4), \quad (2.7)$$

where $p_{ij} = p_{ji} = \vec{\mu}_{1i} \cdot \vec{\mu}_{1j} / |\vec{\mu}_{1i}||\vec{\mu}_{1j}|$ denotes the alignment of the dipole moment matrix elements $\vec{\mu}_{1i}$ and $\vec{\mu}_{1j}$. These damping terms, which are of central importance in this work, arise if quantum interference from spontaneous emission channels from the closely spaced levels are involved. The interference of the three decay processes among themselves are governed by the p_{ij} terms. $p_{ij}=0$ corresponds to the case with no interference whereas $p_{ij}=1$ stands for maximum interference between the spontaneous emissions from $|i\rangle \rightarrow |1\rangle$ and $|j\rangle \rightarrow |1\rangle$. The time evolution for the density-matrix elements in the rotating frame take the form

$$\begin{aligned}\frac{\partial \rho_{44}}{\partial t} = {} & -\gamma_4 \rho_{44} - \gamma_{43}(\rho_{34} + \rho_{43}) - \gamma_{42}(\rho_{24} + \rho_{42}) \\ & - i\Omega_4(\rho_{14} - \rho_{41}), \end{aligned}$$

$$\begin{aligned}\frac{\partial \rho_{33}}{\partial t} = {} & -\gamma_3 \rho_{33} - \gamma_{32}(\rho_{32} + \rho_{23}) - \gamma_{43}(\rho_{43} + \rho_{34}) \\ & - i\Omega_3(\rho_{13} - \rho_{31}), \end{aligned}$$

$$\begin{aligned}\frac{\partial \rho_{22}}{\partial t} = {} & -\gamma_2 \rho_{22} - \gamma_{42}(\rho_{42} + \rho_{24}) - \gamma_{23}(\rho_{32} + \rho_{23}) \\ & - i\Omega_2(\rho_{12} - \rho_{21}), \end{aligned}$$

$$\begin{aligned}\frac{\partial \rho_{41}}{\partial t} = {} & -\left(\frac{\gamma_4}{2} + i\Delta_4\right)\rho_{41} - \gamma_{43}\rho_{31} - \gamma_{42}\rho_{21} + i\Omega_4(\rho_{44} - \rho_{11}) \\ & + i\Omega_3\rho_{43} + i\Omega_2\rho_{42}, \end{aligned}$$

$$\begin{aligned}\frac{\partial \rho_{42}}{\partial t} = {} & -\left(\frac{\gamma_2 + \gamma_4}{2} + i\omega_{42}\right)\rho_{42} - \gamma_{23}\rho_{43} - \gamma_{43}\rho_{32} \\ & - \gamma_{42}(\rho_{22} + \rho_{44}) + i\Omega_2\rho_{41} - i\Omega_4\rho_{12}, \end{aligned}$$

$$\begin{aligned}\frac{\partial \rho_{43}}{\partial t} = {} & -\left(\frac{\gamma_3 + \gamma_4}{2} + i\omega_{43}\right)\rho_{43} - \gamma_{32}\rho_{42} - \gamma_{42}\rho_{23} \\ & - \gamma_{34}(\rho_{33} + \rho_{44}) + i\Omega_3\rho_{41} - i\Omega_4\rho_{13}, \end{aligned}$$

$$\begin{aligned}\frac{\partial \rho_{32}}{\partial t} = {} & -\left(\frac{\gamma_2 + \gamma_3}{2} + i\omega_{32}\right)\rho_{32} - \gamma_{42}\rho_{34} - \gamma_{43}\rho_{42} \\ & - \gamma_{32}(\rho_{22} + \rho_{33}) + i\Omega_2\rho_{31} - i\Omega_3\rho_{12}, \end{aligned}$$

$$\begin{aligned}\frac{\partial \rho_{21}}{\partial t} = {} & -\left(\frac{\gamma_2}{2} + i\Delta_2\right)\rho_{21} - p_{42}\gamma_{42}\rho_{41} - p_{32}\gamma_{32}\rho_{31} \\ & + i\Omega_2(\rho_{22} - \rho_{11}) + i\Omega_4\rho_{24} + i\Omega_3\rho_{23}, \end{aligned}$$

$$\begin{aligned}\frac{\partial \rho_{31}}{\partial t} = {} & -\left(\frac{\gamma_3}{2} + i\Delta_3\right)\rho_{31} - \gamma_{32}\rho_{21} - \gamma_{43}\rho_{41} + i\Omega_3(\rho_{33} - \rho_{11}) \\ & + i\Omega_2\rho_{32} + i\Omega_4\rho_{34}. \end{aligned} \quad (2.8)$$

When arriving at Eq. (2.8), we have used the normalization condition $\rho_{44}+\rho_{33}+\rho_{22}+\rho_{11}=1$ for a closed system. We define the vector $\vec{B}(t)$ given by

$$\begin{aligned}\vec{B}(t) = {} & [\langle\sigma_{41}(t)\rangle, \langle\sigma_{14}(t)\rangle, \langle\sigma_{42}(t)\rangle, \langle\sigma_{24}(t)\rangle, \langle\sigma_{43}(t)\rangle, \langle\sigma_{34}(t)\rangle, \\ & \langle\sigma_{31}(t)\rangle, \langle\sigma_{13}(t)\rangle, \langle\sigma_{21}(t)\rangle, \langle\sigma_{12}(t)\rangle, \langle\sigma_{32}(t)\rangle, \\ & \langle\sigma_{23}(t)\rangle, \langle\sigma_{44}(t)\rangle, \langle\sigma_{33}(t)\rangle, \langle\sigma_{22}(t)\rangle]^T, \end{aligned} \quad (2.9)$$

thus the equation of motion (2.8) can be written in matrix form:

$$\frac{d\vec{B}(t)}{dt} = L_0 \vec{B} + \vec{C}, \quad (2.10)$$

L_0 being a 15×15 matrix whose explicit expression can be easily derived out from the homogeneous part of Eq. (2.8) and the inhomogeneous term $\vec{C}$ in Eq. (2.10) is a column vector whose nonzero components are $C_1 = i\Omega_4$, $C_2 = -i\Omega_4$, $C_7 = i\Omega_3$, $C_8 = -i\Omega_3$, $C_9 = i\Omega_2$, and $C_{10} = -i\Omega_2$.

We proceed to analyze the role of quantum interference on the resonance fluorescence spectrum (RFS). It is well known that this spectrum is proportional to the Fourier transformation of the steady-state correlation function $\lim_{t\rightarrow\infty}\langle E^-(r,\tau+t)E^+(r,t)\rangle$ [3], where $E^-(r,t)/E^+(r,t)$ is the negative/positive frequency part of the radiation field in the far zone. The radiation field consists of a free-field operator and a source-field operator that is proportional to the atomic polarization operator. Therefore the RFS can be expressed in terms of the atomic correlation function,

$$S(\omega) = \text{Re}\left[\int_0^\infty \lim_{t\rightarrow\infty}\langle D^+(\tau+t)D^-(t)\rangle e^{-i\omega\tau} d\tau\right], \quad (2.11)$$

where Re denotes the real part and $D^{\pm}(t)$ is the atomic polarization operator,

$$D^+(t) = \vec{\mu}_{14}\sigma_{41}(t) + \vec{\mu}_{13}\sigma_{31}(t) + \vec{\mu}_{12}\sigma_{21}(t), \quad (2.12)$$

$$D^-(t) = \vec{\mu}_{14}\sigma_{14}(t) + \vec{\mu}_{13}\sigma_{13}(t) + \vec{\mu}_{12}\sigma_{12}(t). \quad (2.13)$$

In the following analysis, we abbreviate $\omega-\omega_L$ by ω, but we should interpret ω as a frequency measured relative to the laser frequency ω_L. We are only interested in the incoherent part of the RFS, $S_{inc}(\omega)$, which is given by

$$S_{inc}(\omega)=\mathrm{Re}\left[\int_0^\infty \lim_{t\to\infty}\langle \Delta D^+(\tau+t)\Delta D^-(t)\rangle e^{-i\omega\tau}d\tau\right], \tag{2.14}$$

where $\Delta D^{\pm}(\tau)=D^{\pm}(\tau)-\langle D^{\pm}(\infty)\rangle$ stands for the deviation of the dipole polarization operator from its mean steady-state value,

$$\begin{aligned}S_{inc}(\omega)=\mathrm{Re}\Bigg(\int_0^\infty [&\mu_{14}^2\langle\Delta\sigma_{41}(\tau)\Delta\sigma_{14}(0)\rangle\\&+\vec{\mu}_{14}\cdot\vec{\mu}_{13}\langle\Delta\sigma_{41}(\tau)\Delta\sigma_{13}(0)\rangle\\&+\vec{\mu}_{14}\cdot\vec{\mu}_{12}\langle\Delta\sigma_{41}(\tau)\Delta\sigma_{12}(0)\rangle\\&+\mu_{13}^2\langle\Delta\sigma_{31}(\tau)\Delta\sigma_{13}(0)\rangle\\&+\vec{\mu}_{13}\cdot\vec{\mu}_{14}\langle\Delta\sigma_{31}(\tau)\Delta\sigma_{14}(0)\rangle\\&+\vec{\mu}_{13}\cdot\vec{\mu}_{12}\langle\Delta\sigma_{31}(\tau)\Delta\sigma_{12}(0)\rangle\\&+\mu_{12}^2\langle\Delta\sigma_{21}(\tau)\Delta\sigma_{12}(0)\rangle\\&+\vec{\mu}_{12}\cdot\vec{\mu}_{14}\langle\Delta\sigma_{21}(\tau)\Delta\sigma_{14}(0)\rangle\\&+\vec{\mu}_{12}\cdot\vec{\mu}_{13}\langle\Delta\sigma_{21}(\tau)\Delta\sigma_{13}(0)\rangle]e^{-i\omega\tau}d\tau\Bigg).\end{aligned} \tag{2.15}$$

The two-time correlation functions are calculated in the Appendix where the final form of the spectrum is provided.

Based in the Bloch equations (2.8) we may also compute the squeezing spectrum. For this purpose, the operator of the electric field at the observation point $\vec{r}$ is required. We introduce a slowly varying electric-field operator with phase θ as

$$\begin{aligned}\vec{E}_\theta(\vec{r},t)&=\frac{1}{2}\vec{E}_\theta^+(\vec{r},t)e^{i(\omega_L t+\theta)}+\frac{1}{2}\vec{E}_\theta^-(\vec{r},t)e^{-i(\omega_L t+\theta)}\\&=\vec{E}_1(\vec{r},t)\cos\theta+\vec{E}_2(\vec{r},t)\sin\theta,\end{aligned} \tag{2.16}$$

where

$$\vec{E}_1(\vec{r},t)=\frac{1}{2}\vec{E}_\theta^+(\vec{r},t)e^{i\omega_L t}+\frac{1}{2}\vec{E}_\theta^-(\vec{r},t)e^{-i\omega_L t}, \tag{2.17}$$

$$\vec{E}_2(\vec{r},t)=\frac{i}{2}\vec{E}_\theta^+(\vec{r},t)e^{i\omega_L t}-\frac{i}{2}\vec{E}_\theta^-(\vec{r},t)e^{-i\omega_L t} \tag{2.18}$$

are the in-phase and out-of-phase quadratures of the fluorescent field relative to the coherent driving field, respectively.

Since we are considering a nearly degenerate atomic system, we could assume that $\omega_{43}\simeq\omega_{32}$. Thus by considering the observation direction to be perpendicular to the atomic dipole moments ($\vec{\mu}_{14}$, $\vec{\mu}_{13}$, and $\vec{\mu}_{12}$), the positive frequency part of the fluorescent field at the detector position takes the form [5]

$$\vec{E}_\theta^+(\vec{r},t)=f(r)[\vec{\mu}_{14}\sigma_{14}(t')+\vec{\mu}_{13}\sigma_{13}(t')+\vec{\mu}_{12}\sigma_{12}(t')]e^{-i\omega_L t'}, \tag{2.19}$$

where $f(r)=\omega_{31}^2/c^2r$, and $t'=t-r/c$.

The normally ordered squeezing spectrum of the fluorescence of the electric-field quadrature component $\vec{E}_\theta$ can be expressed as [55,56]

$$\langle:S_\theta(\vec{r},t,\theta):\rangle=\frac{1}{2\pi}\int_{-\infty}^{\infty}d\tau e^{-i\omega\tau}\langle:\vec{E}_\theta(\vec{r},t),\vec{E}_\theta(\vec{r},t+\tau):\rangle, \tag{2.20}$$

where $\langle A,B\rangle=\langle A.B\rangle-\langle A\rangle\langle B\rangle$. Inserting the positive and negative parts of the fluorescent field given by Eq. (2.19) into Eq. (2.20), we can express the squeezing spectrum in terms of the two-time correlations of the atomic transition operators in the following form:

$$\begin{aligned}\langle:S_\theta(\vec{r},t,\theta):\rangle=\frac{f(r)^2}{4\pi}\,\mathrm{Re}\int_{-\infty}^{\infty}d\tau e^{i\omega\tau}[&(\mu_{12}^2\langle\sigma_{12}(t+\tau),\sigma_{12}(t)\rangle+\vec{\mu}_{12}\cdot\vec{\mu}_{14}\langle\sigma_{12}(t+\tau),\sigma_{14}(t)\rangle+\vec{\mu}_{12}\cdot\vec{\mu}_{13}\langle\sigma_{12}(t+\tau),\sigma_{13}(t)\rangle\\&+\vec{\mu}_{13}\cdot\vec{\mu}_{14}\langle\sigma_{13}(t+\tau),\sigma_{14}(t)\rangle+\mu_{13}^2\langle\sigma_{13}(t+\tau),\sigma_{13}(t)\rangle+\vec{\mu}_{13}\cdot\vec{\mu}_{12}\langle\sigma_{13}(t+\tau),\sigma_{12}(t)\rangle+\mu_{14}^2\langle\sigma_{14}(t+\tau),\sigma_{14}(t)\rangle\\&+\vec{\mu}_{14}\cdot\vec{\mu}_{13}\langle\sigma_{14}(t+\tau),\sigma_{13}(t)\rangle+\vec{\mu}_{14}\cdot\vec{\mu}_{12}\langle\sigma_{14}(t+\tau),\sigma_{12}(t)\rangle)e^{i(2\theta+\omega_L r/c)}+\mu_{14}^2\langle\sigma_{41}(t+\tau),\sigma_{14}(t)\rangle\\&+\vec{\mu}_{14}\cdot\vec{\mu}_{13}\langle\sigma_{41}(t+\tau),\sigma_{13}(t)\rangle+\vec{\mu}_{14}\cdot\vec{\mu}_{12}\langle\sigma_{41}(t+\tau),\sigma_{12}(t)\rangle+\vec{\mu}_{13}\cdot\vec{\mu}_{14}\langle\sigma_{31}(t+\tau),\sigma_{14}(t)\rangle+\mu_{13}^2\langle\sigma_{31}(t+\tau),\sigma_{13}(t)\rangle\\&+\vec{\mu}_{13}\cdot\vec{\mu}_{12}\langle\sigma_{31}(t+\tau),\sigma_{12}(t)\rangle+\vec{\mu}_{12}\cdot\vec{\mu}_{14}\langle\sigma_{21}(t+\tau),\sigma_{14}(t)\rangle+\vec{\mu}_{12}\cdot\vec{\mu}_{13}\langle\sigma_{21}(t+\tau),\sigma_{13}(t)\rangle+\mu_{12}^2\langle\sigma_{21}(t+\tau),\sigma_{12}(t)\rangle].\end{aligned} \tag{2.21}$$

In order to evaluate numerically the squeezing spectrum, one needs to know the atomic two-time correlation functions appearing in Eq. (2.21). This can be accomplished by invoking the quantum regression theorem. In the numerical analysis we will assume $e^{2i\omega r/c}=1$, and will scale the squeezing spectrum by $\mu_{13}^2 f^2(r)/2\pi\gamma$.

Finally we also address the problem of analyzing the susceptibility of a weak, tunable probe field transmitted by the system. The angular frequency of the driving field ω_L is kept fixed, and the probe susceptibility is measured as a function of the angular frequency ω of the probe field, whose susceptibility is proportional to

$$A(\omega) = \int_0^\infty \lim_{t\to\infty}[\langle D^-(t+\tau), D^+(t)\rangle] e^{-i\omega t'} d\tau, \quad (2.22)$$

which can be obtained by means of the quantum regression theorem, in a similar way as the resonance fluorescence spectrum. Note that in Eq. (2.22) $\mathrm{Re}[A(\omega)]/\mathrm{Im}[A(\omega)]$ refers to the absorptive/dispersive part of the linear susceptibility of the probe beam.

III. NUMERICAL RESULTS

The set of density-matrix equations (2.8) can be numerically solved to obtain the time evolution and steady-state values of populations and coherences. In the following we assume that $\gamma_4=\gamma_3=\gamma_2\equiv\gamma$, and the dipoles of the excited states to ground state $\vec{\mu}_{14}$, $\vec{\mu}_{13}$, and $\vec{\mu}_{12}$, to be equal in magnitude and different directions. When the dipolar moments are parallel among them $p_{ij}\equiv p=1$, and consequently $\Omega_2=\Omega_3=\Omega_4\equiv\Omega$.

A. Populations dynamics

First of all, we will analyze how quantum interference modifies the temporal dynamics of populations and coherences. Let us compare the time evolution of the total upper level population $\Sigma\equiv\rho_{44}+\rho_{33}+\rho_{22}$, with the lower level population ρ_{11}. We assume that $\rho_{11}(0)=1$ as the initial condition. In Fig. 2 we plot the time evolution of Σ and ρ_{11} when a moderate external field ($\Omega=0.4\gamma$) is tuned to the intermediate upper level $|3\rangle$. It is seen in Fig. 2(a) that, in the absence of quantum interference ($p=0$), the population mainly remains at the ground level [$\Sigma(\infty)\approx 0.3987$]. Note also that the time required to arrive at steady state is in the order of $10/\gamma$. However, in the presence of maximal quantum interference ($p=1$), the total population in all the upper levels is around $\Sigma(\infty)\approx 0.9739$ [see Fig. 2(b)]. Furthermore, the time required to reach the steady state is in the order of $1000/\gamma$, thus the presence of quantum interference strongly slows down the process of arriving at the steady state. The enlengthment is accompanied by long-lived population oscillations of small amplitude between upper levels $|4\rangle$ and $|3\rangle$ which are in phase opposition to population oscillations between upper levels $|3\rangle$ and $|2\rangle$. The coherent population oscillations vanish after a few oscillations in the absence of quantum interference at an instant of time in the order of $10/\gamma$.

To deeply investigate the effects of the vacuum induced coherence on the total population $\Sigma(\infty)$, we plot in Fig. 2(c) the steady-state population versus p, while keeping $\Omega=0.4\gamma$. It can be seen that $\Sigma(\infty)$ decreases monotonically with p in the range $0<p<0.84$, and passes through a minimum value. This feature suggests that a constructive interference between the different pathways takes place, producing an enhancement of the spontaneous emission which manifests in the depopulation of upper levels in comparison to the case with $p=0$. However, in the range $0.84<p\leqslant 1$, the behavior of the total upper-level population $\Sigma(\infty)$ changes dramatically. In this case, destructive interference is the origin of the depression in the spontaneous emission which manifests in the high values of $\Sigma(\infty)$ obtained. The reason for this will become apparent in Sec. III B. It is also remarkable that the inversion is established even for a weak Rabi frequency ($\Omega=0.4\gamma$). In addition, we have checked numerically that the inversion is only achieved when the degree of quantum interference of the different interfering pathways takes values close to unity simultaneously. In summary, a high degree of quantum interference is essential for the obtention of inversion in the bare basis.

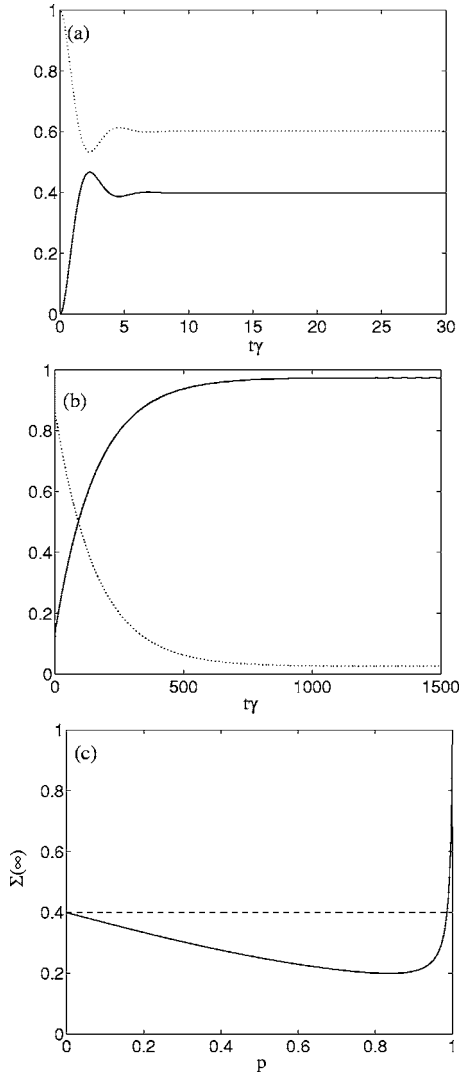

FIG. 2. Time evolution of population of the excited levels Σ (solid line) and the ground level ρ_{11} (dotted line). (a) $p=0$ and (b) $p=1$. (c) Steady-state population of upper states [$\Sigma(\infty)$] as a function of the degree of quantum interference p (solid line). The dashed line indicates $\Sigma(\infty)$ when $p=0$. We assume $\omega_{43}=\omega_{32}=0.1\gamma$, $\Delta_3=0$, and $\Omega=0.4\gamma$.

B. Resonance fluorescence spectrum

Now we turn our attention to the influence of quantum interference on RFS. In Fig. 3 we plot the RFS for different Rabi frequencies when the driving field is tuned to the intermediate level $|3\rangle$ and $\omega_{43}=\omega_{32}=0.1\gamma$. This situation is of

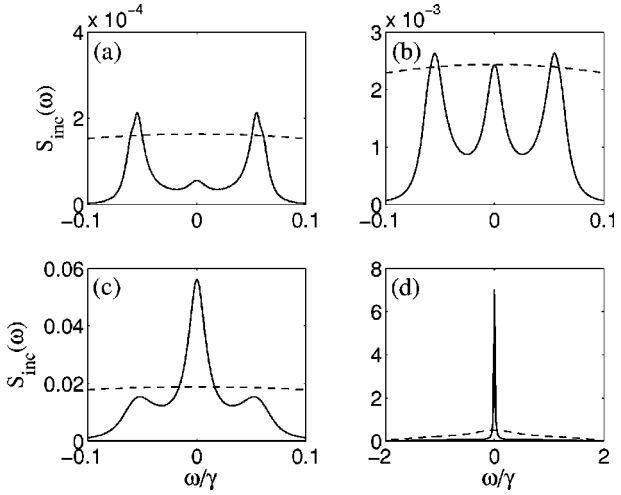

FIG. 3. The two-dimensional incoherent fluorescence spectrum $S_{inc}(\omega)$ as a function of ω, in the case of $\omega_{43}=\omega_{32}=0.1\gamma$ and $\Delta_3=0$. (a) $\Omega=0.02\gamma$; (b) $\Omega=0.04\gamma$; (c) $\Omega=0.07\gamma$; (d) $\Omega=0.4\gamma$. Dashed and solid lines correspond to $p=0$ and $p=0.995$, respectively.

particular interest since, as we will show later, it allows to work out the analytical study in the dressed-state picture. The dashed and solid curves correspond to the cases with $p=0$ and $p=0.995$, respectively. In the absence of quantum interference ($p=0$) and in the range of Rabi frequencies considered here, the spectrum displays a Lorentzian line shape whose width is of the order of γ. However, the spectrum is dramatically modified when spontaneous generated coherence is accounted for. In the case of a very low Rabi frequency $\Omega=0.03\gamma$ the broad emission line splits into two prominent sidebands located near $\omega\approx 0.05\gamma$, indicating a dramatic reduction in the width of the sidebands [see solid line in Fig. 3(a)]. Note also the presence of the central peak with a reduced peak amplitude. When the Rabi frequency is slightly increased the spectrum becomes clearly triple peaked, all lines being subnatural, as it is seen in Fig. 3(b). This fact clearly illustrates that if spontaneous generated coherence is present, the change in the Rabi frequency produces a line narrowing at the central line, and most interestingly, we obtain spectral features that otherwise does not become observable. By further increasing the Rabi frequency the three-peaked structure collapses into a narrow central line where a linewidth of $\Delta\omega\approx\gamma/45$ is obtained [solid line in Fig. 3(d)]. An explanation of these features can be given in terms of the dressed states of the atom, as we will show below. In summary, there is clear evidence that interference arising from the different decay channels substantially modifies the spectral characteristics of the fluorescent field in four-level atoms.

A rich variety of ultranarrow emission peaks can be obtained in different situations. Let us consider, for example, the case in which two of the three upper levels, $|2\rangle$ and $|3\rangle$, are degenerated, the splitting being $\omega_{43}=0.2\gamma$, and the laser field is tuned to the degenerated upper levels. In this configuration we have found similar results to those shown in Fig. 3. However, in the regime of high Rabi frequencies ($\Omega=1\gamma$) an ultranarrow central line is obtained in the presence of quantum interference. This line is a superposition of four Lorentzians with different widths and heights (not shown). In order to get ultranarrow emission lines with appreciable peak intensities, an adequate selection of the Rabi frequency of the driving field must be done. In Fig. 4(a) we plot the peak intensity $S_{inc}(0)$ as a function of the Rabi frequency of the driving field (Ω) while Fig. 4(b) presents the half width at half height ($\Delta\omega$) versus Ω. In the range of moderate Rabi frequencies $\Omega<0.8\gamma$ a reduction in the linewidth is accompanied by an increment of the peak emission intensity, whereas for large Rabi frequencies a further reduction of the linewidth is obtained at the expense of obtaining low peak intensities.

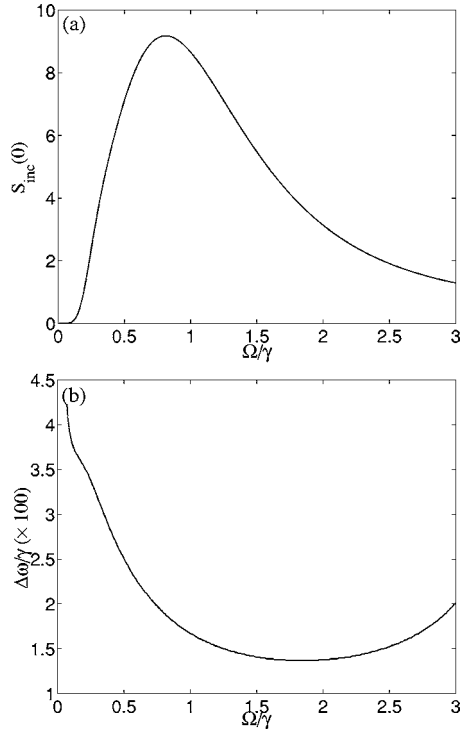

FIG. 4. (a) Peak emission of the incoherent fluorescence spectrum $S_{inc}(0)$ as a function of Ω. (b) Full width at half height ($\Delta\omega$) of the central peak as a function of Ω. The upper levels $|2\rangle$ and $|3\rangle$ are degenerated and $\omega_{43}=0.2\gamma$. The external field is tuned to the degenerated upper levels and $p=0.995$.

Ultranarrow peaks arising from quantum interference have been previously reported in other atomic systems such as V-type atoms [41]. We must stress that the simultaneous linewidth reduction preserving the peak intensity has been successfully accomplished by Keitel [53] with an ingenious proposal consisting of a four-level scheme driven by a coherent field and different incoherent pumping rates. The price to pay for maintaining the peak emission intensity, is the use of a strong coherent field and a rather involved pumping schema. The major challenge of the system considered in this work is that similar narrowing of the spectral lines can be obtained with a single and moderate driving field and without incoherent pumping. The peak emission intensities obtained in our scheme remain appreciable even for the cases with extreme subnatural linewidths.

Some of the results obtained numerically in this section can be interpreted in the atom-field dressed representation. It

is well known that positions, widths, and heights of resonance fluorescence peaks can be understood through energies, electronic dipole moments, and steady-state populations of dressed states [54]. In order to obtain the dressed states under arbitrary parametric conditions, we have to resort to numerical methods due to the high complexity of the equations of the atomic system. However, under special circumstances we can look for analytical solutions. This case corresponds to the physical situation considered in Fig. 3, where $\Delta_3=0$ and $\Delta_4=-\Delta_2$. The dressed states are obtained by finding the eigenvectors of the coherent part of the interaction Hamiltonian, Eq. (2.5), i.e., we must solve

$$H_{ext}|\psi_i\rangle = \lambda_i|\psi_i\rangle \quad (i=1,2,3,4), \tag{3.1}$$

where the eigenstates can be written in terms of the bare states as

$$|\psi_i\rangle = C_{i1}|1\rangle + C_{i2}|2\rangle + C_{i3}|3\rangle + C_{i4}|4\rangle. \tag{3.2}$$

In this situation, the coefficients C_{ij} in Eq. (3.2) are

$$C_{i1} = \frac{\lambda_i(\lambda_i+\Delta_4)\Omega}{D_i}, \quad C_{i2} = \frac{\lambda_i\Omega^2}{D_i},$$

$$C_{i3} = \frac{(\lambda_i+\Delta_4)\Omega^2}{D_i},$$

$$C_{i4} = \frac{\lambda_i^2(\lambda_i+\Delta_4) - \Omega^2\lambda_i - \Omega^2(\lambda_i+\Delta_4)}{D_i}, \tag{3.3}$$

D_i being

$$D_i = \sqrt{[(\lambda_i+\Delta_4)^2(\lambda_i^2+\Omega^2) + \Omega^2\lambda_i^2]\Omega^2 + [(\lambda_i+\Delta_4)(\lambda_i^2-\Omega^2) - \Omega^2\lambda_i]^2}, \tag{3.4}$$

and the corresponding eigenvalues λ_i are such that $\lambda_4=-\lambda_1=\sqrt{x_+}$ and $\lambda_3=-\lambda_2=\sqrt{x_-}$, where

$$x_\pm = \frac{1}{2}[(3\Omega^2+\Delta_4^2) \pm \sqrt{(3\Omega^2+\Delta_4^2)^2 - 4\Delta_4^2\Omega^2}]. \tag{3.5}$$

In order to explain the widths of the resonance fluorescence peaks, we calculate the rate of transition from $|\psi_i\rangle$ to $|\psi_j\rangle$, which is proportional to the squared dipole moment $R_{ij}=|\langle\psi_j|P_1|\psi_i\rangle|^2$ where $P_1=\vec{\mu}_{14}|1\rangle\langle 4| + \vec{\mu}_{13}|1\rangle\langle 3| + \vec{\mu}_{12}|1\rangle\langle 2|$ is the transition dipole moment operator. R_{ij} is explicitly given by

$$\begin{aligned} R_{ij} &= |\langle\psi_j|P_1|\psi_i\rangle|^2 \\ &= |C_{j1}|^2[\mu_{14}^2|C_{i4}|^2 + \mu_{13}^2|C_{i3}|^2 + \mu_{12}^2|C_{i2}|^2 + I_i] \\ &\quad (i,j=1,2,3,4), \end{aligned} \tag{3.6}$$

and I_i read as

$$I_i = 2p(C_{i4}C_{i3} + C_{i4}C_{i2} + C_{i3}C_{i2}) \quad (i=1,2,3,4). \tag{3.7}$$

The inspection of Eq. (3.6) reveals that quantum interference strongly modifies the rate of transition due to the presence of the interference term I_i [see Eq. (3.7)]. In fact, when this term takes negative values, the rate R_{ij} can take very low or zero value, and consequently, the transition from state $|\psi_i\rangle$ to state $|\psi_j\rangle$ is unlikely due to the destructive interference. This indicates a slow decay of the corresponding dressed population and consequently a spectral narrowing.

In order to explain the main features of the spectra, we plot in Fig. 5(a) the eigenvalues given by Eq. (3.5), the corresponding schema of the dressed states in Fig. 5(b), the steady-state population of the dressed states in Fig. 5(c), and the interference terms of the rate of transition given by Eq. (3.7) in Fig. 5(d), as a function of the Rabi frequency Ω. Note that the energies of the dressed states $|\psi_2\rangle$ and $|\psi_3\rangle$ depend weakly on Ω [see Fig. 5(a)]. In fact the energy difference between the two eigenstates is $\lambda_3-\lambda_2\simeq 0.05\gamma$. This value corresponds to the frequency of the sidebands displayed in Figs. 3(a)–3(c). Moreover, in the regime of low Rabi frequency, $0<\Omega<0.07\gamma$, most of the population accu-

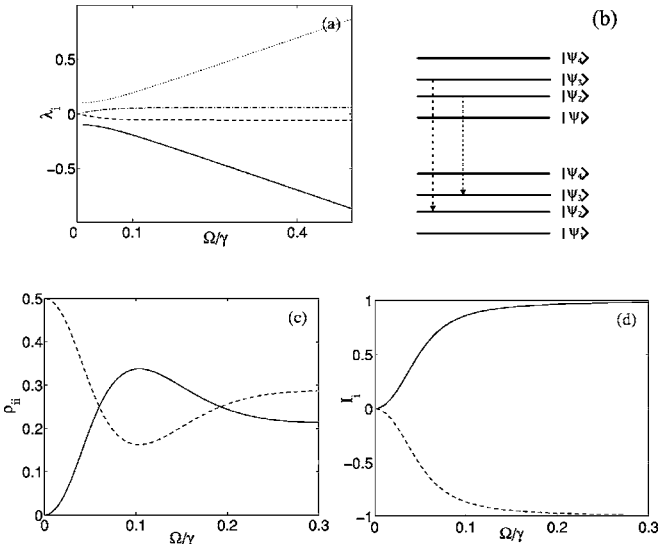

FIG. 5. (a) The eigenvalues given by Eq. (3.5) as a function of Rabi frequency Ω, λ_1 (solid line), λ_2 (dashed line), λ_3 (dashed-dotted line), and λ_4 (dotted line). (b) The corresponding schema of the dressed states indicating the relevant transitions that produce the sidebands shown in Figs. 3(a)–3(c). (c) Steady-state population of the dressed states as a function of Rabi frequency Ω, $\rho_{\psi_1\psi_1}=\rho_{\psi_4\psi_4}$ (solid line), and $\rho_{\psi_2\psi_2}=\rho_{\psi_3\psi_3}$ (dashed line). (d) The interference terms of the rate of transition given by Eq. (3.7) as a function of the Rabi frequency Ω, $I_1=I_4$ (solid line), and $I_2=I_3$ (dashed line). The parameters used are $p=0.995$, $\omega_{43}=\omega_{32}=0.1\gamma$, and $\Delta_3=0$.

mulates in the dressed states $|\psi_2\rangle$ and $|\psi_3\rangle$. This explains the appearance of the two peaks in Figs. 3(a)–3(c) which arises from transitions from $|\psi_2\rangle$ to $|\psi_3\rangle$ and from $|\psi_3\rangle$ to $|\psi_2\rangle$ [indicated by the vertical dashed arrows in Fig. 5(b)]. The central peak can be attributed to transitions from $|\psi_3\rangle$ to $|\psi_3\rangle$ and from $|\psi_2\rangle$ to $|\psi_2\rangle$ since the other two transitions ($|\psi_1\rangle \rightarrow |\psi_1\rangle$ and $|\psi_4\rangle \rightarrow |\psi_4\rangle$) do not significantly contribute to this central frequency, due to the low level of population in states $|\psi_1\rangle$ and $|\psi_4\rangle$, according to the curves displayed in Fig. 5(c). All the above-mentioned transitions take place with and without quantum interference, although the emergence of subnatural peaks only becomes observable in the presence of a high degree of quantum interference. The reason lies in the strong narrowing experienced by these emissions lines due to destructive quantum interference. This can be concluded from a single inspection of Fig. 5(d) where the interference terms I_3 and I_2 of the rate of transitions R_{32}, R_{23}, R_{33}, and R_{22} exhibit negative values, which is an indication of slow decays in comparison to the case with $p=0$. At higher Rabi frequencies, $\Omega > 0.07\gamma$, all the dressed states are populated [see Fig. 5(c)]. In this situation, the central line is contributed by all the four possible transitions [$|\psi_i\rangle \rightarrow |\psi_i\rangle (i=1,2,3,4)$], thus the amplitude of the central peak becomes much larger than the amplitudes of the sidebands [see Fig. 3(c)] and eventually make them unobservable [see Fig. 3(d)].

To further explore the origin of the low-frequency inner sidebands shown in Figs. 3(a)–3(c), we have analyzed the transient evolution of the population of the dressed states. We have found that the population of all the dressed states oscillates at a frequency of 0.057γ, which is in coincidence with the frequency of the sidebands numerically obtained. It is worth noting that, in the absence of quantum interference ($p=0$), the population of the dressed states evolves monotonically in time. Thus we can conclude that the physical origin of the Rabi sidebands can be attributed to population oscillations induced by quantum interference.

The role of interference effects in the inversion found in Fig. 2(c) can also be addressed by considering the dressed state basis. There we showed how a high degree of quantum interference is essential in order to accumulate most of the population in the upper levels. In fact, for moderate values of p we found that the population in the upper levels is less than that obtained in the absence of quantum interference. The origin of this striking behavior can be made transparent by the simultaneous analysis of the population of the dressed states and the sign of the interference terms I_i of the transitions rates involved. We plot in Fig. 6(a) the steady-state population of the dressed states versus the degree of quantum interference p, while the interference terms of the rate of transition I_i are presented in Fig. 6(b). It is clearly seen that for values of p lesser than 0.9 most of the population accumulates in states $|\psi_1\rangle$ and $|\psi_4\rangle$ (solid line) and the corresponding interference terms ($I_1=I_4$) displayed with solid line in Fig. 6(b) exhibit positive values, i.e., constructive interference takes place as described in Eq. (3.6). This interference produces an enhancement of the spontaneous emission which accounts for the lower values of population of upper states [$\Sigma(\infty)$] in comparison to the case with $p=0$. Whereas for values of p close to unity, the population is transferred to

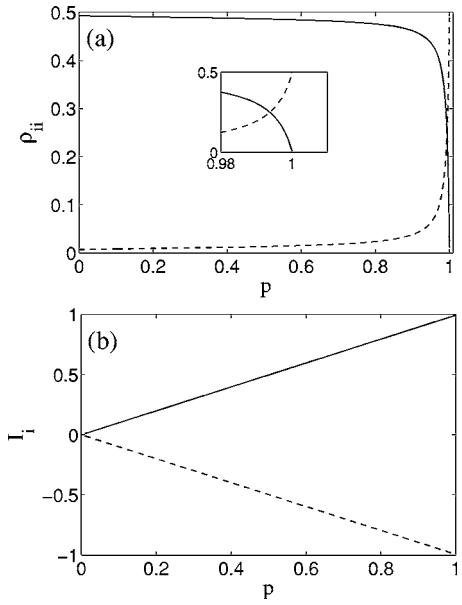

FIG. 6. (a) Steady-state population of the dressed states as a function of p, $\rho_{\psi_1\psi_1}=\rho_{\psi_4\psi_4}$ (solid line), and $\rho_{\psi_2\psi_2}=\rho_{\psi_3\psi_3}$ (dashed line). (b) The interference terms of the rate of transition given by Eq. (3.7), as a function of p, $I_1=I_4$ (solid line) and $I_2=I_3$ (dashed line). The parameters used are $\Omega=0.4\gamma$, $\omega_{43}=\omega_{32}=0.1\gamma$, and $\Delta_3=0$.

dressed states $|\psi_2\rangle$ and $|\psi_3\rangle$. In this case the corresponding interference terms ($I_2=I_3$), displayed with a dashed line in Fig. 6(b), exhibit negative values, i.e., destructive interference takes place as described in Eq. (3.6). In this case population accumulates in the upper states and produces an extreme line narrowing.

C. Phase-dependent resonance fluorescence spectrum

In this section we analyze the role of vacuum induced coherences in the squeezing spectrum. We present in Fig. 7(a) the squeezing spectrum of the out-of-phase quadrature for a symmetric atomic configuration where the splitting between the excited levels are the same. We consider $\omega_{43}=\omega_{32}=0.6\gamma$, and a Rabi frequency $\Omega=0.1\gamma$. The dashed/solid line corresponds to the case without/with quantum interference. The most remarkable effect of quantum interference is the strong enhancement of the squeezing of the fluorescent field around the laser frequency [see solid line in Fig. 7(a)]. Most interestingly, the in-phase quadrature displayed in Fig. 7(b) reveals that squeezing is shifted to the sidebands when quantum interference is accounted for, producing a two-mode squeezed field. It is to be noted that squeezing does not occur at any frequency in the absence of quantum interference [dashed line in Fig. 7(b)]. When considering a large Rabi frequency of the driving field, say for example $\Omega=\gamma$, the fluorescent field does not present a reduction of the fluctuations beyond the standard limit in any quadrature in the absence and in the presence of interference (not shown). The results obtained in the squeezing spectra reveal a remarkable departure from the behavior found in a resonantly driven two-level atom [55] and that found in a V-type atom [56],

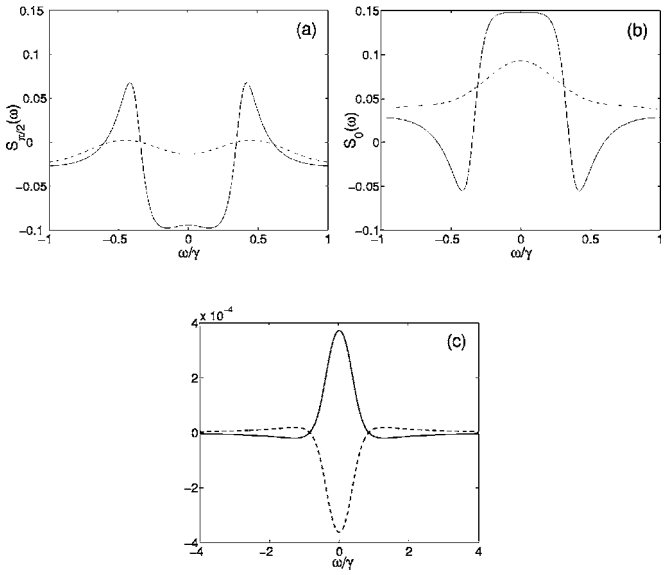

FIG. 7. Squeezing spectra as a function of ω for $\omega_{43}=\omega_{32}=0.6\gamma$, $\Delta_3=0$, $\Omega=0.1\gamma$, $p=0$ (dashed line), and $p=0.995$ (solid line): (a) out-of-phase quadrature and (b) in-phase quadrature. (c) For comparison purposes, we present the squeezing spectra as a function of ω in the case of a V-type atom with two upper levels, $|a\rangle$ and $|b\rangle$, decaying to the common lower level $|1\rangle$ via the same vacuum modes, such that $\omega_{ab}=1.2\gamma$, and the driving field is tuned to the middle of the two upper levels. The Rabi frequency of the driving field is selected to be 0.1γ and the degree of quantum interference is set equal to 0.995 (as in the four level atom considered in this work): out-of-phase quadrature (solid line) and in-phase quadrature (dashed line).

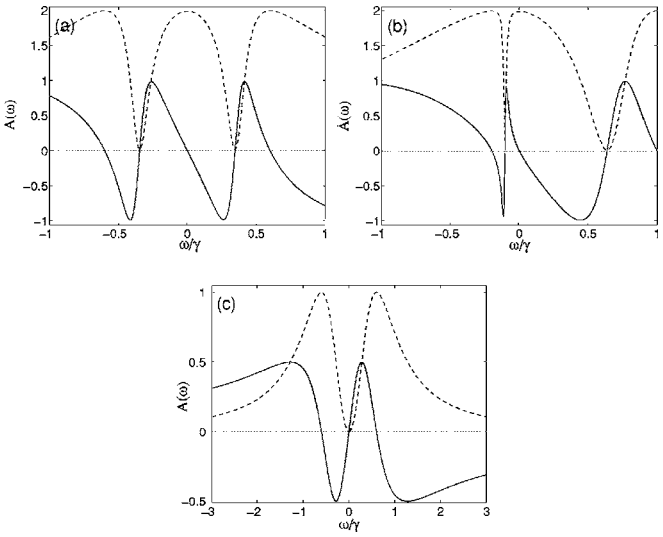

FIG. 8. Imaginary (solid lines) and real (dashed lines) parts of the probe susceptibility $A(\omega)$ as a function of ω. (a) $\omega_{43}=\omega_{32}=0.6\gamma$. (b) $\omega_{43}=1\gamma$, and $\omega_{32}=0.2\gamma$. Other parameters are $\Delta_3=0$, $p=1$, and $\Omega=0.02\gamma$. (c) For comparison purposes, we present the imaginary (solid line) and real (dashed line) parts of the probe susceptibility $A(\omega)$ as a function of ω in the case of a V-type atom with two upper levels, $|a\rangle$ and $|b\rangle$, decaying to the common lower level $|1\rangle$ via the same vacuum modes, such that $\omega_{ab}=1.2\gamma$, and the driving field is tuned to the middle of the two upper levels. The Rabi frequency of the driving field is selected to be 0.02γ and the degree of quantum interference is set equal to unity [as in the four level atom considered (a)].

where the squeezing occurs only in a quadrature. It should be noted that squeezing can also be obtained for other atomic configurations, not only the ones selected to produce Figs. 7(a) and 7(b), i.e., by selecting different frequency separations between the excited levels and/or Rabi frequencies, the fluorescent field presents a notable reduction of the fluctuations when quantum interference is allowed (not shown).

Finally, we must point out that the addition of a four-upper-level to the traditional three-level V-type atom leads to critical differences between the two systems. This is illustrated in Fig. 7(c) where the squeezing spectra for the in-phase/out-of-phase (dashed/solid line) quadrature of a V-type atom is plotted. Note that the in-phase quadrature exhibits an almost zero squeezing around the laser frequency, i.e., the achieved level of reduction of fluctuations is three orders of magnitude lesser in the V-type atom than in the four-level atom considered in this work.

D. Absorption spectrum

Although we have seen that quantum interference modifies both the resonance fluorescence and the squeezing spectra of this atomic system, the most relevant spectral features of this atomic system with regard to the three-level V-type atomic configurations appear when considering the absorption of a weak probe field. Here we show how the presence of quantum interference leads to very interesting phenomena with potential applications in the area of slow light propagation and the entanglement of two photons at different frequencies.

Let us consider the absorption spectrum of a weak, tunable probe field transmitted by the atomic medium. Figure 8(a) shows the susceptibility for a symmetric configuration with $\omega_{43}=\omega_{32}=0.6\gamma$, when the external field is tuned to level $|3\rangle$, i.e., $\Delta_3=0$. We note that two narrow holes appear, that is, the usual dark resonance obtained in a V-type three-level system splits into two holes [57]. Simultaneously, the dispersion curves (see solid lines) present a very high slope at the center of the two transparency windows, so the group velocity can be considerably slowed down. By changing the splitting or the detuning of the driving field, the absorption spectrum can be made different at the two holes, as displayed in Fig. 8(b) where we present the absorption for an asymmetric configuration with $\omega_{43}=1\gamma$, $\omega_{32}=0.2\gamma$, and $\Delta_3=0$. In summary, the more appealing result is the appearance of a double hole bored into the broad spectrum. It is worth mentioning that the spectrum is very broad in the absence of quantum interference.

The peculiarities concerning the absorption spectra can be explained by looking at the linear-response regime. In this regime, where the probe laser-atom interaction is weak, Eqs. (2.8) may be linearized by assuming that for weak laser fields ρ_{11} remains essentially constant and nearly equal to unity, thus $\rho_{22}\approx\rho_{33}\approx\rho_{44}\approx 0$, while the only evolving quantities are coherences ρ_{21}, ρ_{31}, and ρ_{41}. We assume $p_{ij}=p$. Thus, keeping terms to first order in the field Ω, the linear susceptibility is then given by

$$\chi = 2i \frac{\left(1-p+i\frac{2\Delta_4}{\gamma}\right)\left[2(1-p)+i\frac{2(\Delta_2+\Delta_3)}{\gamma}\right]+\left(1-p+i\frac{2\Delta_2}{\gamma}\right)\left(1-p+i\frac{2\Delta_3}{\gamma}\right)}{\left(1+i\frac{2\Delta_4}{\gamma}\right)\left(1-p+i\frac{2\Delta_3}{\gamma}\right)\left(1-p+i\frac{2\Delta_2}{\gamma}\right)+p\left(1-p+i\frac{2\Delta_4}{\gamma}\right)\left[2(1-p)+i\frac{2(\Delta_2+\Delta_3)}{\gamma}\right]}. \tag{3.8}$$

Expression (3.8) allows us to calculate the position of the two holes where the probe susceptibility nearly vanishes. In the case of maximal quantum interference ($p \simeq 1$), the position of the holes are

$$\omega_{dark} = \frac{(\omega_{43}-\omega_{32})}{3} \pm \frac{1}{3}\sqrt{\omega_{43}^2+\omega_{32}^2+\omega_{43}\omega_{32}}. \tag{3.9}$$

For the case analyzed in Fig. 8(a), i.e., in the symmetrical configuration of the three-upper levels, the holes are symmetrically placed at $\omega_{dark} = \pm\omega_{43}/\sqrt{3} \simeq \pm 0.35\gamma$, in agreement with the result displayed in Fig. 8(a). In the asymmetrical configuration considered in Fig. 8(b), Eq. (3.9) gives 0.64γ and -0.1γ, in agreement with the numerical result.

In the case with maximum quantum interference and when considering the case with $\omega_{43}=\omega_{32}$, the imaginary part of χ can be approximated to

$$\mathrm{Im}(\chi) \approx 2\left[\frac{\gamma^2}{\gamma^2+\Delta_3^2} - \frac{(\omega_{43}/4)^2}{(\omega_{43}/4)^2+[\Delta_3-(\omega_{43}/\sqrt{3})]^2} - \frac{(\omega_{43}/4)^2}{(\omega_{43}/4)^2+[\Delta_3+(\omega_{43}/\sqrt{3})]^2}\right], \tag{3.10}$$

which is adequate in the limit $\omega_{43} \ll \gamma$. Expression (3.10) indicates that the spectrum consists of three Lorentzians, and those with negative weights are responsible for the appearance of the holes bored into the broad absorption spectrum. The widths of the holes represented by the Lorentzians with negative weights are proportional to the splitting ω_{43}, thus the holes can be made very narrow by reducing ω_{43}. For example, in atomic systems composed of atomic hyperfine levels it could possible to modify the level spacing with an external magnetic field.

We also note that the modification to the EIT profile affects the refractive index of the medium. The spectral features appear in the absorption spectrum and are very sharp. This leads to sharp refractive index changes with frequency. We can see that the probe dispersion exhibits a normal steep at the absorption minimum near $\pm\omega_{dark}$, allowing the slowing down light pulses. Furthermore, the four-level atom with vacuum induced coherence supports slow photons at frequencies $\omega \pm \omega_{dark}$ simultaneously. Moreover, the width and the position of the two holes can be controlled with the atomic splitting and the Rabi frequency in order to optimize the group velocity of the pulse. In fact, the narrowing of the holes in the absorption spectrum as described in Eq. (3.10) is of major interest since it allows us to obtain a large and positive slope of the dispersion and, consequently, a great reduction of group velocity of a weak probe pulse. This feature cannot be produced in the usual three-level *V*-type atom as it can be concluded from the inspection of Fig. 8(c). It can be clearly seen that, for the same values of the parameters as in Fig. 8(a), the *V* system shows the usual EIT response with a dip at the two-photon resonant frequency. The holes are a direct consequence of the spontaneous generated coherence. Similar results have been encountered in other four-level configurations such as double Λ [57] or tripod atoms [26,29,58,59]. The main difference is that in the present case, the double hole is generated via spontaneous coherence instead of the dynamically induced coherence.

Using the linear approximation given by Eq. (3.8), we can also compute the slope of the real part of the susceptibility at the hole center. This magnitude plays a crucial role in light propagation since it is proportional to the group index n_g. After some calculation we arrive at the following result:

$$n_g \propto \mathrm{Re}\left(\frac{\partial\chi}{\partial(\omega/\gamma)}\right)_{\omega=\omega_{dark}} = \frac{2\gamma^2(3\omega_{dark}+\omega_{32}-\omega_{43})}{\omega_{dark}^2(2\omega_{dark}+\omega_{32}-\omega_{43})}. \tag{3.11}$$

The index group of Eq. (3.11) is very sensitive to the splitting of the upper levels. The slopes of the dispersive curve at the transparency windows become steeper as ω_{43} and/or ω_{32} decreases leading to an increasingly lower group velocity. In fact, when $\omega_{43}=\omega_{32}$, the two holes are symmetrically placed being their slopes equal to $9\gamma^2/(\omega_{43}^2)$ in agreement with Fig. 8(a). In the case of a *V*-type atom Bortman-Arbiv *et al.* [60] found a similar value for the slope of the dispersion.

Finally we consider the question of how perfect are the transparency windows presented in Figs. 8(a) and 8(b). The numerical analysis reveals that, although in the case of a *V*-type atom the dip in the absorption spectrum presents vanishing absorption at the line center [see Fig. 8(c)], in the four-level atom the transparency windows depart slightly from the perfect EIT condition. For example, in the situation displayed in Fig. 8(a) with equispaced energy levels, the absorption is in the order of 0.0198 and the real part the refractive index is in the order of 0.0068. In the asymmetric configuration considered in Fig. 8(b) the absorption in the right window (0.009) is less than that in the left window (0.153).

IV. CONCLUSIONS

In this paper we have discussed how quantum interference affects the resonance fluorescence, the squeezing, and the absorption spectra and the populations dynamics of a laser driven four-level atom consisting of three closely spaced upper levels decaying to a common lower level. The possibility of decaying to the ground level via the same vacuum modes

allows spontaneously generated coherence to take place. We have found significant population inversion with moderate Rabi frequencies of the driving field. We show that spontaneous generated coherence slows down the process of arriving at the steady state.

We have also analyzed the influence of quantum interference on RFS. Extreme line narrowing at the sidebands and at the central line are obtained simultaneously for moderate Rabi frequencies. An interpretation of the features found in the RFS has been given in terms of the dressed states of the atom.

The influence of quantum interference among the three decay pathways on the squeezed spectrum is analyzed. We find that for weak resonance excitation, squeezing occurs both in the in-phase and the out-of-phase quadratures, a feature which is not present either in two-level atoms or in the usual *V*-type atom in free space. In addition, quantum interference produces a strong enhancement of the squeezing of the fluorescent field. Particularly, the squeezing spectrum in the in-phase quadrature exhibits two-mode squeezing at the Rabi sidebands.

Finally, we have studied the absorption spectrum of a weak tunable probe. The broad spectrum obtained in the absence of quantum interference is bored with two narrow holes when interference is accounted for. The narrowing can be controlled by changing the level splitting. The existence of these holes with large slope of the refractive index may be useful to entangle two slow probe pulses. The spectral properties of the holes could be modified by changing the level spacing.

This rich variety of phenomena may find possible applications in the areas of high-resolution spectroscopy, control of fluorescence at definite frequencies, population transfer, and slow light propagation.

To conclude, we call attention to the condition required to prove experimentally the theoretical results predicted in this work. It is concerned with the requirement that quantum interference between the three decay channels may only occur when the transitions involved are nonorthogonal. There is a principle difficulty in the realization of atomic interference via spontaneous emission for atomic transitions in free space. A number of proposals [61] have been made for explicitly getting around this problem and have been reviewed in an excellent work by Ficek and Swain [4]. Recently, Kocharovskaya *et al.* proposed to take advantage of the technique of photonic band-gap materials and semiconductor quantum dots [62]. Further, in recent years, great efforts have been focused on the engineering of quantum dots with sufficiently close upper levels to allow for spontaneous generated coherence.

ACKNOWLEDGMENT

This work has been supported by the Ministerio de Educacion y Ciencia under Project No. FIS2004-03267 (Spain).

APPENDIX: STEADY-STATE RESONANCE FLUORESCENCE SPECTRUM

The two-time correlation functions that appear in Eq. (2.15) can be obtained by invoking the quantum regression theorem together with the optical Bloch equation (2.8). Thus we define the column vector

$$\begin{aligned}\hat{U}_j = [&\Delta\sigma_{41}(\tau)\Delta\sigma_{1j}(0), \Delta\sigma_{14}(\tau)\Delta\sigma_{1j}(0), \Delta\sigma_{42}(\tau)\Delta\sigma_{1j}(0),\\ &\Delta\sigma_{24}(\tau)\Delta\sigma_{1j}(0), \Delta\sigma_{43}(\tau)\Delta\sigma_{1j}(0), \Delta\sigma_{34}(\tau)\Delta\sigma_{1j}(0),\\ &\Delta\sigma_{31}(\tau)\Delta\sigma_{1j}(0), \Delta\sigma_{13}(\tau)\Delta\sigma_{1j}(0), \Delta\sigma_{21}(\tau)\Delta\sigma_{1j}(0),\\ &\Delta\sigma_{12}(\tau)\Delta\sigma_{1j}(0), \Delta\sigma_{32}(\tau)\Delta\sigma_{1j}(0), \Delta\sigma_{23}(\tau)\Delta\sigma_{1j}(0),\\ &\Delta\sigma_{44}(\tau)\Delta\sigma_{1j}(0), \Delta\sigma_{33}(\tau)\Delta\sigma_{1j}(0), \Delta\sigma_{22}(\tau)\Delta\sigma_{1j}(0)]^T\\ &(j=2,3,4), \end{aligned} \tag{A1}$$

where the superindex T stands for transpose. According to the quantum regression theorem, for $\tau>0$ the vector $\hat{U}_j$ satisfies

$$\frac{d\hat{U}_j}{d\tau} = L_0\hat{U}_j(\tau) \quad (j=2,3,4). \tag{A2}$$

By following the same procedure as described in Ref. [41] and working in Laplace space we obtain the steady-state fluorescence spectrum. Specifically we have

$$\begin{aligned} S_{inc}(\omega) = \mathrm{Re}\Bigg\{ &\sum_{k=1}^{k=15} [\gamma_4 R_{1k}(iz) + \gamma_{43} R_{7k}(iz) + \gamma_{42} R_{9k}(iz)]\hat{U}_4^{(k)}\\ &\times(0) + [\gamma_3 R_{7k}(iz) + \gamma_{43} R_{1k}(iz) + \gamma_{32} R_{9k}(iz)]\hat{U}_3^{(k)}(0)\\ &+ [\gamma_2 R_{9k}(iz) + \gamma_{42} R_{1k}(iz) + \gamma_{32} R_{9k}(iz)]\hat{U}_2^{(k)}(0)\Bigg\}, \end{aligned} \tag{A3}$$

where $\hat{U}_j^{(k)}(0)$ is the steady-state value of the kth component of the vector $\hat{U}_j(t)$. $R_{jk}(iz)$ is the (j,k) element of the matrix $R(iz)$ defined as

$$R(iz) = (iz\hat{I} - L_0)^{-1}, \tag{A4}$$

$\hat{I}$ being the 15×15 identity matrix, and $z \equiv (\omega-\omega_L)/\gamma_4$.

[1] S. E. Harris, Phys. Today **50**(7), 36 (1997).

[2] J. P. Marangos, J. Mod. Opt. **45**, 471 (1998).

[3] M. O. Scully and M. S. Zubairy, *Quantum Optics* (Cambridge University Press, London, 1997).

[4] Z. Ficek and S. Swain, J. Mod. Opt. **49**, 3 (2002).

[5] L. M. Narducci, M. O. Scully, G. L. Oppo, P. Ru, and J. R. Tredicce, Phys. Rev. A **42**, 1630 (1990).

[6] S. E. Harris, J. E. Field, and A. Imamoglu, Phys. Rev. Lett. **64**, 1107 (1990).

[7] K. J. Boller, A. Imamoglu, and S. E. Harris, Phys. Rev. Lett.

66, 2593 (1991).
[8] O. Kocharovskaya and Y. I. Khanin, JETP Lett. **48**, 630 (1988).
[9] S. E. Harris, Phys. Rev. Lett. **62**, 1033 (1989).
[10] M. O. Scully, S-Y. Zhu, and A. Gavrielides, Phys. Rev. Lett. **62**, 2813 (1989).
[11] J. Mompart and R. Corbalán, J. Opt. B: Quantum Semiclassical Opt. **2 R7**, 175 (2000).
[12] M. O. Scully, Phys. Rev. Lett. **67**, 1858 (1991).
[13] S. E. Harris, J. E. Field, and A. Kasapi, Phys. Rev. A **46**, R29 (1992).
[14] M. Fleischhauer, C. H. Keitel, M. O. Scully, Ch. Su, B. T. Ulrich, and S.-Y. Zhu, Phys. Rev. A **46**, 1468 (1992).
[15] M. O. Scully and M. Fleischhauer, Phys. Rev. Lett. **69**, 1360 (1992).
[16] K. Hakuta, L. Marmet, and B. P. Stoicheff, Phys. Rev. Lett. **66**, 596 (1991).
[17] S. E. Harris, Phys. Rev. Lett. **72**, 52 (1994).
[18] E. Paspalakis and P. L. Knight, J. Mod. Opt. **47**, 1025 (2000).
[19] Y.-F. Li, J.-F. Sun, X.-Y. Zhang, and Y.-C. Wang, Opt. Commun. **202**, 97 (2001).
[20] K. T. Kapale, M. O. Scully, S.-Y. Zhu, and M. S. Zubairy, Phys. Rev. A **67**, 023804 (2003).
[21] D. Bullock, J. Evers, and C. H. Keitel, Phys. Lett. A **307**, 8 (2003).
[22] H. Schmidt and A. Imamoglu, Opt. Commun. **131**, 333 (1996); A. D. Greentree, J. A. Vaccaro, S. R. Echaniz, A. V. Durrant, and J. P. Marangos, J. Opt. B: Quantum Semiclassical Opt. **2**, 252 (2000).
[23] P. Grangier, D. F. Walls, and K. M. Gheri, Phys. Rev. Lett. **81**, 2833 (1998).
[24] S. E. Harris and Y. Yamamoto, Phys. Rev. Lett. **81**, 3611 (1998); S. E. Harris and L. V. Hau, *ibid.* **82**, 4611 (1999).
[25] M. Yan, E. G. Rickey, and Y. Zhu, Phys. Rev. A **64**, 041801(R) (2001).
[26] B. S. Ham and P. R. Hemmer, Phys. Rev. Lett. **84**, 4080 (2000).
[27] B. S. Ham, Appl. Phys. Lett. **78**, 3382 (2001).
[28] A. Zibrov, M. D. Lukin, L. Hollberg, and M. O. Scully, Phys. Rev. A **65**, 051801(R) (2002).
[29] S. Rebic, D. Vitali, C. Ottaviani, P. Tombesi, M. Artoni, F. Cataliotti, and R. Corbalán, Phys. Rev. A **70**, 032317 (2004).
[30] M. D. Lukin and A. Imamoglu, Phys. Rev. Lett. **84**, 1419 (2000).
[31] J. Wang, Yifu Zhu, K. J. Jiang, and M. S. Zhan, Phys. Rev. A **68**, 063810 (2003).
[32] D. Petrosyan and G. Kurizki, Phys. Rev. A **64**, 023810 (2001).
[33] G. S. Agarwal, *Quantum Optics*, Springer Tracts in Modern Physics Vol. 70 (Springer-Verlag, Berlin, 1974).
[34] G. S. Agarwal, Phys. Rev. A **18**, 1490 (1978).
[35] B. M. Garraway and P. L. Knight, Phys. Rev. A **54**, 3592 (1996).
[36] S.-Y. Zhu, L. M. Narducci, and M. O. Scully, Phys. Rev. A **52**, 4791 (1995).
[37] S.-Y. Zhu, and M. O. Scully, Phys. Rev. Lett. **76**, 388 (1996).
[38] E. Arimondo, Prog. Opt. **35**, 257 (1996).
[39] H. Lee, P. Polynkin, M. O. Scully, and S.-Y. Zhu, Phys. Rev. A **55**, 4454 (1997).
[40] P. Zhou and S. Swain, Phys. Rev. Lett. **77**, 3995 (1996).
[41] P. Zhou and S. Swain, Phys. Rev. A **56**, 3011 (1997).
[42] F. Carreño, M. A. Antón, and O. G. Calderón, Opt. Commun. **221**, 365 (2003).
[43] D. A. Cardimona, M. G. Raymer, and C. R. Stroud, J. Phys. B **15**, 55 (1982).
[44] E. Paspalakis and P. L. Knight, Phys. Rev. Lett. **81**, 293 (1998).
[45] E. Paspalakis, N. J. Kylstra, and P. L. Knight, Phys. Rev. Lett. **82**, 2079 (1999).
[46] U. Akram, Z. Fizek, and S. Swain, J. Mod. Opt. **48**, 1059 (2001).
[47] M. A. Antón and O. G. Calderón, J. Opt. B: Quantum Semiclassical Opt. **4**, 91 (2002).
[48] M. A. Antón, O. G. Calderón, and F. Carreño, Phys. Lett. A **311**, 297 (2003).
[49] V. A. Malyshev, F. Carreño, M. A. Antón, O. G. Calderón, and F. Domínguez-Adame, J. Opt. B: Quantum Semiclassical Opt. **5**, 313 (2003).
[50] M. A. Antón, O. G. Calderón, and F. Carreño, Phys. Rev. A **69**, 023801 (2004).
[51] A. Joshi, W. Yang, and M. Xiao, Phys. Lett. A **325**, 30 (2004).
[52] M. Fleischhauer and M. D. Lukin, Phys. Rev. A **65**, 022314 (2001).
[53] C. H. Keitel, Phys. Rev. Lett. **83**, 1307 (1999).
[54] C. Cohen-Tannoudji, J. Dupont-Roc, and G. Grynberg, *Atom-Photon Interactions* (Wiley, New York, 1992).
[55] M. J. Collet, D. F. Walls, and P. Zoller, Opt. Commun. **52**, 145 (1984).
[56] Shao-yan Gao, Fu-li Li, and Shi-yao Zhu, Phys. Rev. A **66**, 043806 (2002).
[57] M. D. Lukin, S. F. Yelin, M. Fleischhauer, and M. O. Scully, Phys. Rev. A **60**, 3225 (1999).
[58] E. Paspalakis and P. L. Knight, J. Opt. B: Quantum Semiclassical Opt. **4**, S372 (2002).
[59] D. Petrosyan and Y. P. Malakyan, Phys. Rev. A **70**, 023822 (2004).
[60] D. Bortman-Arbiv, A. D. Wilson-Gordon, and H. Friedmann, Phys. Rev. A **63**, 043818 (2001).
[61] A. K. Patnaik and G. S. Agarwal, Phys. Rev. A **59**, 3015 (1999); Z. Ficek and S. Swain *ibid.* **69**, 023401 (2004).
[62] O. Kocharovskaya, A. B. Matsko, and Y. Rostovtsev, Phys. Rev. A **65**, 013803 (2001).